Real-Time Voltage Security Assessment using Synchrophasors

Vaithianathan "Mani" Venkatasubramanian
School of EECS, Washington State University
Pullman WA 99164-752
Email: mani@eecs.wsu.edu

Abstract

Voltage stability has played a major role in at least two of the recent major blackouts in North America, namely, July 2, 1996 Western American blackout, and August 14, 2003 Northeastern blackout. Voltage instability phenomena were encountered in these two blackouts because reactive power supplies such as generator reactive power outputs and shunt capacitor devices were exhausted ahead of the eventual blackouts. This paper provides new tools for real-time Voltage Security Assessment (VSA) monitoring that exploit the local nature of the voltage stability problem. The paper proposes algorithms for quantifying the voltage instability margins in terms of reactive power loading limits. The algorithms pinpoint the critical parts of the power system in the context of voltage security in real time operating environment. The paper describes the new algorithms together with illustrative examples on the IEEE 30 bus and 300 bus standard test systems. The algorithms facilitate fast computation of the QV margins at any bus in the system. The algorithms estimate static voltage stability limits by predictively identifying the exhaustion of reactive power supplies under load variations.

Key words: Voltage stability, voltage security, reactive power management, synchrophasors.

1. Introduction

Voltage instability phenomena have played major roles in the occurrence of many recent blackouts. There exists a rich history of publications on voltage stability analysis methods in power systems (for instance, see [1], [2], [3]). While the theoretical analysis of voltage stability is relatively well understood, there exist only a few computational tools for monitoring and mitigating voltage instability phenomena in real-time operational environment. This paper focuses on fast real-time detection of static voltage stability problem that is related to the existence (or non-existence) of power-flow solutions for a power system model under quasi-steady state conditions. Two algorithms are presented for quantifying the voltage security status of the operating condition, and the algorithms also identify potential problem areas that are prone to static voltage instability. The algorithms are motivated by the emerging large-scale implementations of synchrophasors in power systems all over the world whereby the power-flow state of the system will be available in real-time. The algorithms can also be implemented in present day power systems by using combinations of both slow SCADA measurements and fast synchrophasor measurements.

There are fundamental differences between the flow of active versus reactive power in power transmission networks, which must be kept in mind in deriving voltage stability tools for monitoring and control. Unlike active power, which can flow from sources to sinks over long transmission paths, reactive power needs to be supplied and balanced locally to meet the reactive power demands at load centers. Reactive power losses over transmission lines and transformers are typically several factors higher than active power losses. It is well known that voltage stability phenomena tend to be local while active power phenomena may involve geographically widespread operational domains. The algorithms proposed in the paper exploit the local nature of the reactive power flow problem by intelligent book-keeping of reactive power sources and sinks in calculating the static limits of operation.

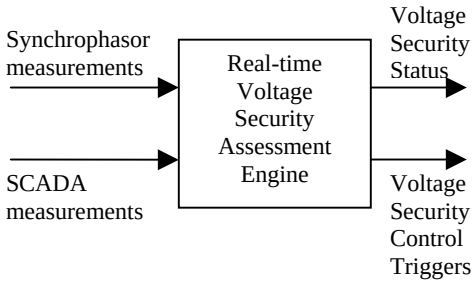

Figure 1.1 Real-time Voltage Security Controller

The objectives of real-time security controller shown in Figure 1.1 are a) to monitor the status of voltage security of a power system, and b) to initiate suitable control measures such as switching of transformer banks and/or capacitor/reactor banks, as well as shedding of loads whenever necessary to mitigate an

impending voltage stability problem. The inputs to the real-time voltage security assessment engine could include both the traditional SCADA measurements as well as fast synchrophasor measurements. The algorithms presented in Sections 5 and 6 of this paper serve as the computational engines of the voltage security assessment controller. Whenever the security margins, as computed in Sections 5 and 6, fall below certain pre-specified thresholds, the controller in Figure 1.1 can be programmed to initiate specific control actions which will be discussed in future publications.

The paper is organized as follows. Basic power system concepts are introduced in Section 2. Power-flow analysis is formulated in Section 3. Section 4 discusses an example of static voltage stability analysis. Sections 5 and 6 present two new algorithms for fast calculation of voltage instability margins.

2. Fundamental concepts of electrical power

Let us consider a simple AC circuit of a load drawing an AC current *i(t)* from a circuit node that has an AC voltage *v(t)*, where *v(t)* and *i(t)* are of the form,

$$\begin{aligned} v(t) &= \sqrt{2}V\cos(wt) \\ i(t) &= \sqrt{2}I\cos(wt-\varphi) \end{aligned} \quad (1.1)$$

For steady state analysis, the circuit variables can be represented by their respective phasors $\boldsymbol{V}$ and $\boldsymbol{I}$ where $\boldsymbol{V} = V\angle 0$ and $\boldsymbol{I} = I\angle -\varphi$. Then, the instantaneous power $p(t)=v(t)i(t)$ drawn by the load can be simplified into the form

$$\begin{aligned} p(t) &= 2VI\cos(wt)\cos(wt-\varphi) \\ &= P(1+\cos 2wt)+Q\sin 2wt \end{aligned} \quad (1.2)$$

where $P = VI\cos\varphi$ and $Q = VI\sin\varphi$. From Equation (1.2), it is clear that P is the average value of the instantaneous power $p(t)$ over one time period. P is defined as the active power or real power or average power in standard textbooks. The other term Q denotes the amplitude of the swinging second power component in Equation (1.2). Q is usually called as the reactive power. Next, we define the complex phasor power $\boldsymbol{S}$ by $\boldsymbol{S} = \boldsymbol{V}\boldsymbol{I}^*$ so that P is the real part of $\boldsymbol{S}$ and Q is the imaginary part of $\boldsymbol{S}$.

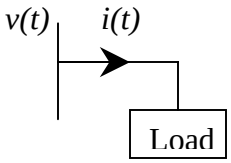

Figure 1.1 A simple illustration of an AC load

To understand the differences between active and reactive power, let us assume the load to be pure impedance. We will study the three basic types of ideal loads, namely, resistive, inductive and capacitive loads.

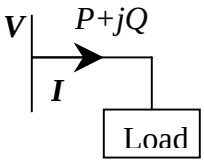

Figure 1.2 Phasor representation

a) *Resistive load:* Suppose $\boldsymbol{I} = \boldsymbol{V}/R_L$ where R_L is the load resistance. Then, it is easy to see that $P = V^2/R_L$, and $Q=0$. That is, the resistive load is a pure active power load and consumes no reactive power.
b) *Inductive load:* Suppose $\boldsymbol{I} = \boldsymbol{V}/(j\,X_L)$, where $X_L = wL$ is the reactance of the inductive load. Then, we get $P = 0$ and $Q = V^2/X_L = I^2 X_L$. We conclude that an inductive load does not consume any active power since $P=0$. Moreover, since the current arrow in Figure 1.2 is pointing into the load and the sign of Q is positive, we say that an inductive load is consuming reactive power or that it is a sink for reactive power.
c) *Capacitive load:* Suppose $\boldsymbol{I} = \boldsymbol{V}(j\,B_C)$ where $B_C = wC$ is the susceptance of the capacitor. We compute $P =0$ and $Q = -V^2 B_C$. Here we note that the sign of Q is negative while being a load, which indicates that the reactive power Q is flowing out of a capacitive load in Figure 1.2. Therefore, we say that a capacitive load supplies reactive power to the grid, or that it acts like a source of reactive power in AC circuits.

In power transmission networks, both real and reactive power-flows must be fully balanced throughout the transmission network under steady-state operating conditions. For active power, generators act as sources while loads throughout the power grid together with active power losses in power grid equipment serve as real power sinks. Efficient designs of power system equipment such as transformers and transmission lines have been historically emphasized to ensure low active power losses in transmitting the real power from generators to loads.

Similarly, the loads mostly act as reactive power sinks in the power system. Moreover, majority of the power grid equipment such as transformers and transmission lines contain mostly reactance in their circuit representations, and hence they act as reactive power consumption devices. In a typical power system, it is impossible to supply all of the reactive power demands from generators alone. Therefore, mostly shunt and

some series capacitor banks are installed throughout the power system to act as additional reactive power sources. In summary, reactive power outputs of synchronous generators and shunt/series capacitive devices need to be balanced with the reactive power consumption of loads as well as other reactive power sinks to ensure reliable steady state operation.

The electrical designs of transformers and transmission lines are inherently such that their reactances are five to ten times as much as their resistances in the circuit representation. These devices, prevalent in modern day power systems, incur five to ten times more reactive power losses compared to active power losses. In other words, the reactive power-flow problem deals with a highly lossy transmission system while the active power-flow deals with a relatively lossless transmission system. Since the active power losses are relatively low compared to reactive power losses, it is possible to transmit active power over long geographical distances in an economically viable fashion. On the other hand, reactive power demands need to be met locally near the loads to ensure efficient reactive power management. In the next section, we will see that both active and reactive power problems are also coupled together and are nonlinear which makes the problem theoretically challenging.

Under heavy loads, the reactive demands on a generator can become so high that the field circuit in some synchronous generator can get overheated. To prevent permanent damage to the field circuit, field over-current limiters then reduce the field current of the overheated unit, thus leading to a sudden drop in the reactive power output of that generator. Since the reactive power balance must be always balanced, the drop in reactive power output of one generator must be compensated by an increase in the reactive power outputs of neighboring generators, and their field circuits can subsequently become overheated. Such cascading reduction of reactive power outputs from several generators near load centers can lead to a cascading reduction of transmission system voltages in the area and the phenomenon is known as the *classical voltage collapse* problem. The declining voltages typically lead to high line currents thus leading to cascading line outages, load and generator trippings and a possible electric blackout.

The aim of this paper is to develop fast algorithms for detecting power-flow related static voltage collapse phenomena in large electric power systems.

3. Review of power-flow equations

Let us consider the power transmission network shown in Figure 3.1.

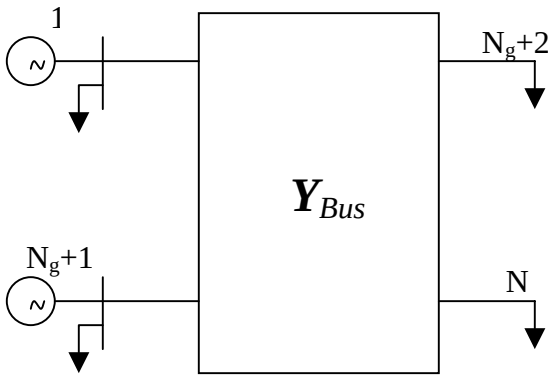

Figure 3.1 Electric power transmission network

At each bus say bus i, we assume the presence of a generator, load and a set of transmission lines connected to a few other buses in the network.

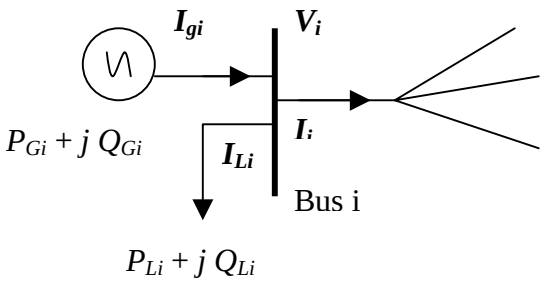

Figure 3.2 Power balance at bus I

Assuming that an RLC circuit represents each transmission line, the admittance matrix YBus below can describe the relationship between bus voltage phasors Vi and current injection phasors Ii:

$$\begin{bmatrix} V_1 \\ \cdot \\ \cdot \\ \cdot \\ V_N \end{bmatrix} = \underline{Y}_{Bus} \begin{bmatrix} I_1 \\ \cdot \\ \cdot \\ \cdot \\ I_N \end{bmatrix} \qquad (2.1)$$

Representing the (i,j)-th entry of $\underline{Y}_{Bus}$ as $Y_{ij} = Y_{ij} \angle \gamma_{ij}$, and $V_i = V_i \angle \delta_i$, we can derive the power balance equations at each bus to be

$$P_i = P_{Gi} - P_{Li} = \sum_{j=1}^{N} Y_{ij} V_i V_j \cos(\delta_i - \delta_j - \gamma_{ij}) \quad (3.2)$$

$$Q_i = Q_{Gi} - Q_{Li} = \sum_{j=1}^{N} Y_{ij} V_i V_j \sin(\delta_i - \delta_j - \gamma_{ij}) \quad (3.3)$$

Under steady state conditions, power-flow equations (3.2) and (3.3) must be satisfied at each bus for normal operation of the power system. There are two equality constraints (3.2) and (3.3) at each bus. There are four variables P_i, Q_i, V_i and δ_I at each bus. Two of the four variables are usually specified or known at each bus, and we can solve for the remaining two from the equations (3.2) and (3.3). The equations (3.2) and (3.3) are clearly nonlinear and the equations are also coupled across all buses, and hence, the solution of the power-flow equations is nontrivial.

In formulating the power-flow problem, we divide the buses into three types, namely, 1) slack bus, 2) PV bus, and 3) PQ bus. We will introduce the reasoning for the names briefly. We assume that the real power outputs of the generator P_{Gi} for all the buses, and both the real and reactive power loads P_{Li} and Q_{Li} at all the buses to be specified. PV bus normally hosts a generator so that the generator field exciter controls automatically maintain the bus voltage V_i at a pre-specvified value V_i^{ref} subject to bounds on the reactive power output Q_{Gi} of the generator. That is, as long as Q_{Gi} stays above a minimum value $Q_{Gi}^{\min}$ and a maximum value Q_{Gi}^{max}, the bus voltage is assumed to be at the speccified value V_i^{ref}. If the reactive power output Q_{Gi} either goes below the lower limit $Q_{Gi}^{\min}$ or goes above the upper limit Q_{Gi}^{max}, we formulate the reactive power output Q_{Gi} to be stuck the respective limiting value and the voltage V_i is no longer at the specified value V_i^{ref}.

We assume that the real power outputs of the generator P_{Gi} for all the buses, and both the real and reactive power loads P_{Li} and Q_{Li} at all the buses to be specified. Therefore, the real power injection P_i=P_{Gi}-P_{Li} is known at the generator bus as well as the bus voltage V_i. Since P and V quantities are known at the bus, the bus with the generator is usually called a *PV bus*. On the other hand, at a load bus or at a generator bus where the Q_G limits are exceeded, the real and reactive power injection P_i and Q_i are specified and such a bus is then denoted a *PQ bus*.

In solving the equations, the overall power conservation must be always preserved. That is, the total power generated must equal the total power consumed for the entire network for both real and reactive power. It turns out that we have to include an ideal generator bus or a slack bus that behaves like an ideal voltage source with unlimited real and reactive power capacity to account for modeling errors while preserving the power conservation law. This type of ideal voltage source accounts for all the slack in real and reactive power errors in the system and is denoted a *slack bus*.

A typical power system such as the western American power system consists of several thousands of buses. Therefore, the solution of the power-flow problem involves finding the simultaneous solution of a large set of the nonlinear power-flow equations (3.1) and (3.2). Standard numerical algorithms such as Newton-Raphson method together with specialized power system algorithms such as the fast-decoupled algorithm are used to solve the equations. The coupling of the unknown variables V_i and δ_i in equations (3.1) and (3.2) is highly sparse which helps the computational algorithms. Details on the algorithms can be seen in standard power engineering textbooks ([4],[5]).

4. Illustration of voltage instability in a 39 bus system

In this section, we will study the classical slow voltage instability phenomenon in a standard 39 bus test system and overview the current tools used by the industry for its analysis. In the next section, we propose fast approximate algorithms for speeding up the analysis in a real-time computational environment.

The power-flow data for the New England test system is available at the website [6]. There are ten generators in the system, marked G1 through G10 in Figure 4.1.

When we solve the base-case power-flow for the loads and generations as shown in the appendix, we note that the reactive power outputs of the three generators G4, G5 and G6 are all at their maximum values. Therefore, the generator buses 33, 34 and 36 are treated as PQ buses in solving the power-flow. This indicates that the system may be stressed in terms of meeting the relative power demands in this part of the grid. If the system is stressed further, there is a danger that the reactive power problems become worse, possibly leading to voltage collapse or voltage instability scenario.

To analyze the potential vulnerability of the system towards voltage collapse, we will analyze the system using QV plots. Let us randomly choose bus 24 that is close to generators G4, G5 and G6. We will gradually increase the reactive power load at bus 24 and study the power-flow solutions. The plot of reactive load Q_{L24} versus the bus voltage V_{24} is shown in Figure 4.2.

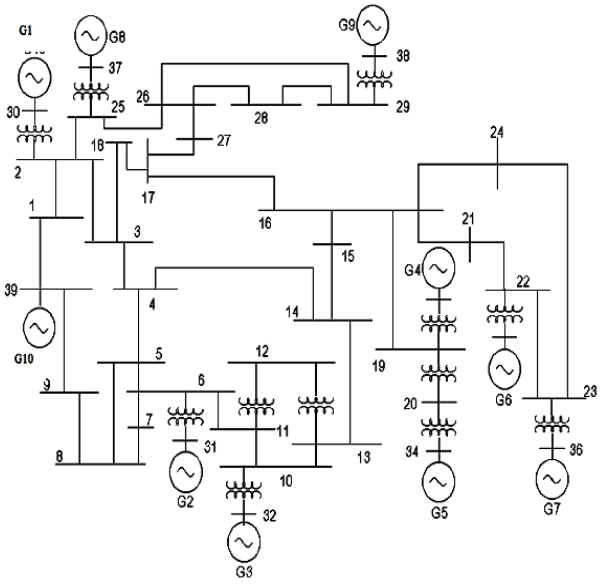

Figure 4.1 New England 39 bus test system

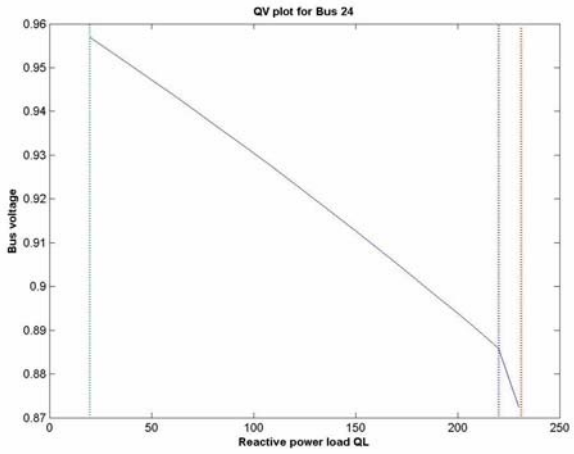

Figure 4.2 QV plot for Bus 24

When the reactive power load Q_{L24} at Bus 24 is increased from the base-case value of 20 MVAR, it can be seen that the voltage V_{24} at Bus 24 continues to decrease. When the load Q_{L24} reaches 220 MVAR, the reactive power output of the generator G7 reaches its maximum limit and the bus 36 becomes a PQ bus. At this point, all the other generators nearby, namely, generators G4, G5, G6 and G7 have reached their maximum reactive power capacity and are unable to provide any higher reactive power outputs in the power-flow problem. Even though the remaining generators, namely, G1, G2, G3, G8, G9 and G10, have plenty of reactive power reserves still available, the reactive power losses in the transmission paths from these distant generators to the stressed Bus 24 complicate the reactive power balancing near Bus 24. In fact, when the reactive power load Q_{L24} goes above 230 MVAR, there is no solution to the power-flow problem. In other words, the power system in Figure 4.1 cannot operate in steady state fashion under the assumptions of the power-flow problem formulation. The limiting value for Q_{L24} = 230 MVAR denotes *a static operating limit* for the solution of the power-flow equations (2.1) and (2.2) for our system. We say that the static limit value Q_{L24} = 230 MVAR defines an *operating boundary* for the *static voltage collapse* phenomenon. Reflecting back to the base-case load value of Q_{L24} = 20 MVAR at Bus 24, we say that the difference between the static limit value of 230 MVAR and the base-case load value of 20 MVAR, that is, 210 MVAR, is denoted the QV margin at Bus 24.

To study the reactive power stress levels in different parts of the system, we will next repeat the QV plot procedure from above at each of the 39 buses in the system. For each Bus i, we will gradually increase the reactive power load Q_{Li} at Bus i alone until the power-flow fails to converge. Then, the QV margin at bus i would be the difference between the static limit of the reactive power load Q_{Li} and the base-case reactive power load Q_{Li} at Bus i. Figure 4.3 shows the QV margins for each of the 39 buses.

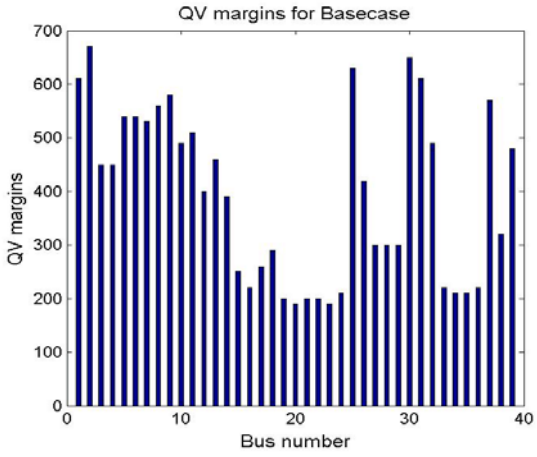

Figure 4.3 QV margins

From the analysis, the lowest QV margin is observed at Bus 20 with a value of 190 MVAR. In fact, all the buses near bus 20 including Bus 24 have QV margins near 200 MVAR. This indicates that this region of the system near generators G4, G5 and G6 is the most stressed with respect to the voltage stability problem.

Loss of transmission lines from contingencies or outages can further aggravate the reactive power

problems. As an illustration, let us assume that the transmission line connecting Buses 23 and 24 has been disconnected for routine maintenance while the generation and load levels are the same as in the study above. For the system after the outage of the transmission line between Buses 23 and 24, the QV margins are shown in Figure 4.4. The QV margins are much lower in Figure 4.4 compared to the values in Figure 4.3. Specifically, the QV margins have decreased down to 50 MVAR after the line outage at many buses near Bus 24, while their values were near 200 MVAR in Figure 4.3 when the line was in service. Low values of the QV margins near 50 MVAR in the region near Bus 24 in Figure 4.3 imply that the system is voltage insecure after the outage of the line connecting Buses 23 and 24. With the line out of service, even a small increase in the loads at any of the buses near Bus 24 could render the operation outside the static limit, possibly leading to slow voltage collapse in the region.

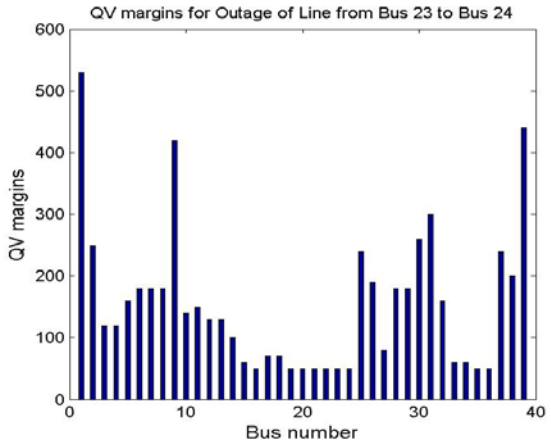

Figure 4.4 QV margins after Line outage

In summary, it is important that any power system must have sufficient reactive power reserves to withstand load increases as well as contingencies without facing the danger of voltage instability by going outside static operating limits. QV plots and QV margins are useful tools to judge the voltage security of the system and to quantify the stress level of the system with respect to voltage instability. They can also be used to locate the problematic regions of the system that are vulnerable to voltage instability. There are other power-flow based tools including PV plots and other load scaling studies, which are used in the power industry for voltage stability studies and they are similar to the QV plot approach introduced above.

On the other hand, while the QV plot based approach discussed in this section is popular in the industry and is a powerful tool, the process of repeated computation of the power-flow solutions is time-consuming. This is especially true if the QV margins need to be recomputed after a large number of transmission line outages and generator outages. Because of the computational burden, the QV plot approach is mostly used for off-line planning studies in the power industry in the present day power system.

QV analysis of the July 2, 1996 WECC blackout that was related to voltage instability can be seen in [7].

For real-time operational tools, we need fast techniques for estimating the QV margins at different buses without having to do a continuum of power-flow solutions as is usually done previously. In the next section, we propose new algorithms for fast computation of QV static limits by heuristic analysis.

5. Fast Predictive QV Margin Calculator

In this section, we propose the first of new algorithms for fast calculation of QV curves and the QV margins that were introduced in Section 4. Both algorithms employ much fewer power-flow computations as compared to traditional algorithms in the literature, and they are motivated towards real-time implementations.

The first algorithm in Section 5.1 is an *accelerated predictive* implementation of the traditional power-flow algorithm that has been custom developed for computing the QV margins rapidly. The algorithm uses a small number of repeated power-flow runs to estimate the QV margins by using a predictive approach. The algorithm can be interfaced with any of the standard power-flow engines in the market. We will illustrate the algorithm using the Matlab based Matpower power-flow toolbox that is available as a freeware power-flow program from the PSerc website [8]. Extensive power-flow simulations of the 39 bus New England test system show that the algorithm gives excellent and fast approximations of the QV margins for diverse operating conditions and contingencies.

The second algorithm in Section 6 directly computes an approximation of a QV margin for any bus from a solved power-flow solution by processing the power-flow Jacobian matrix and the generator Q reserves. It is extremely fast to implement and provides a reasonable approximation of the QV margins especially for the cases when the margins are low. It is designed to be a fast early warning type algorithm for detecting the proximity to potential voltage instability phenomena so that suitable control measures can be initiated to mitigate the problem.

We will illustrate the algorithm in this section for the computation of QV margin at any bus. The algorithm can be easily extended for computing other type of voltage stability power-flow tools including PV curves, area load scaling studies etc.

Suppose we want to find the QV margin at bus i, and the starting value for the reactive power load at bus i is Q_{Li}^{0}. We start with $\Delta Q_{Li}=0$. The objective is to compute the QV margin Q_{Li}^{margin} at bus i so that the load value of $Q_{Li}=Q_{Li}^{0}+Q_{Li}^{margin}$ will correspond to the static limit or the nose of the QV curve. The algorithm presented below computes the values of Q_{Li}^{margin} at each bus in the system without carrying out a continuum of large number of power-flow solutions.

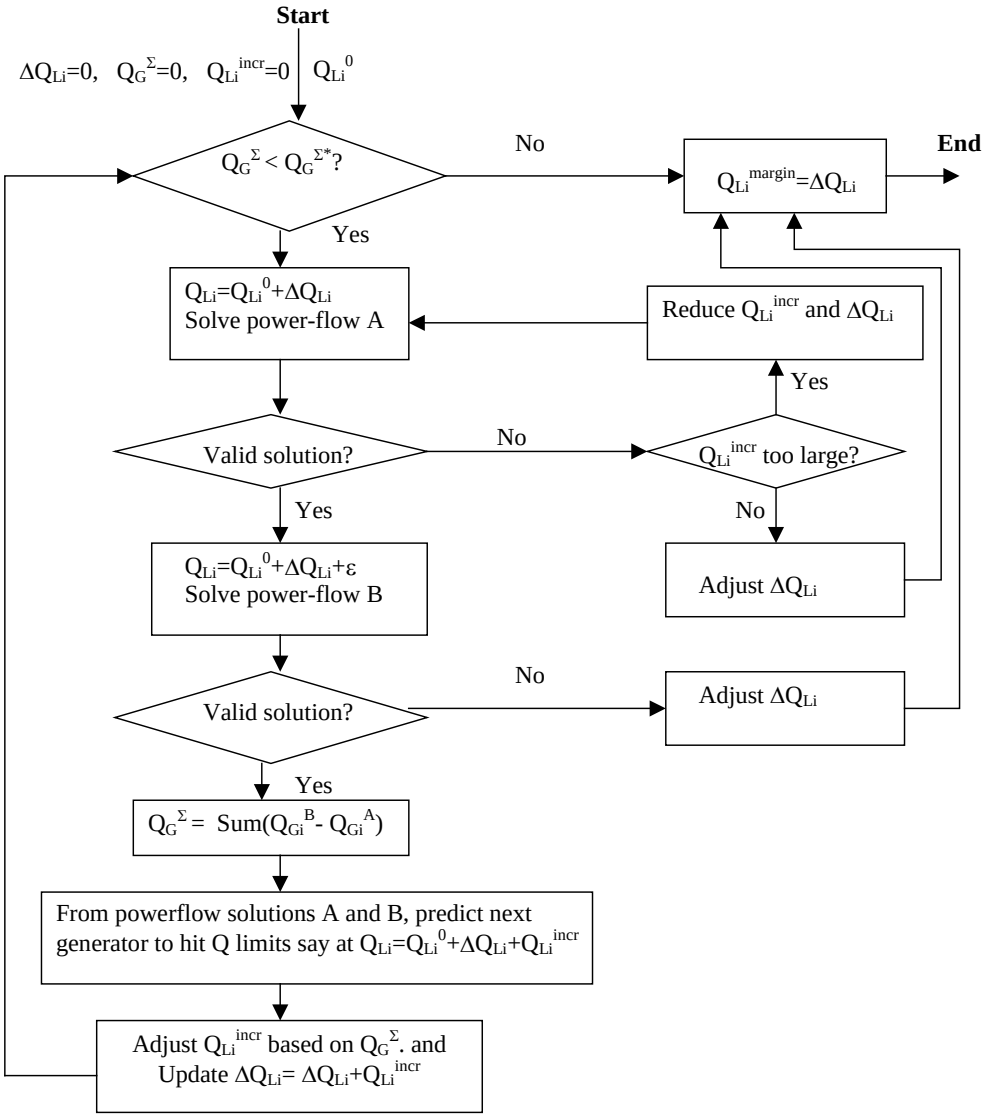

Figure 5.1. Flow-chart of Fast Predictive QV Margin Calculator

5.1 Fast Predictive QV Margin Calculator Algorithm:

The algorithm is summarized in Figure 5.1. In the flowchart, there are two power-flow solutions denoted Solution A and B at each iteration. Using the two solutions, the algorithm then computes or predicts the value of the reactive power load Q_{Li} when the next generator is likely to hit the maximum limit of its reactive power output. If one of the two power-flow solutions fails to converge in any step, the lack of existence of power-flow solution implies that the reactive power loading of Q_{Li} is beyond the static limit and the limiting value is adjusted accordingly. The flow of the iterations is controlled by a measure called Q_G^{Σ}, which is defined as the sensitivity of the net change in generation Q outputs to an incremental change in Q_{Li}. It is claimed that Q_G^{Σ} stays near one for lightly loaded conditions and increases well above one when the system approaches static limits. Therefore, the value of Q_G^{Σ} is used as a measure of proximity to the static limit in the algorithm of Figure 5.1. In the simulations that follow later in this section, we show that the algorithm does work well for standard IEEE test systems.

5.2 Test results for the 39 bus system

In this section, we will test the algorithm of Figure 5.1 on the New England 39 bus system that was introduced in Section 4. In the following simulations, we use the values of 10 MVAR for ε, and 3 for $Q_G^{\Sigma *}$. Figure 5.2 shows a comparison of the QV margins computed by traditional repeated power-flow computational procedure (denoted Actual with solid bars) versus the approximate values (denoted Approx with shaded bars) of our Fast Predictive Algorithm. The QV margins denoted Actual in Figure 5.2 are calculated to an accuracy of 10 MVAR, which was the step size for repeated power-flow simulations. Clearly, the QV margins match well for all the 39 buses in Figure 5.2. The maximum differences between the actual and approximate values occur at Bus 8 where approximate margin is lower than the actual margin by 27 MVAR, and at Bus 6 where the approximate margin is more than the Actual margin by a rather negligible 2 MVAR. Note that the Actual QV margins range from 190 MVAR at Buses 20 and 23 to 670 at Bus 2. The average error between the actual and approximate QV margins over the 39 buses is only 10 MVAR. The approximate values computed by the fast algorithm match the actual values over the entire range of QV margins. Also, the results of the fast predictive algorithm are mostly conservative as compared to the actual values in Figure 5.2.

The number of power-flow solutions needed to compute the approximate QV margins of Figure 5.1 depends on the size of QV margin itself. More specifically, the number of iterations for the fast predictive algorithm is proportional to the number of generators that reach their Q limits along the QV plot. Figure 5.3 shows a plot of the number of iterations of the fast algorithm together with respective computed QV margins at the buses. There are usually two power-flow computations in each iteration excepting near the static limit as shown in Figure 5.1. The average value of the number of iterations is 3.6 over all the 39 buses. The iterations vary between a minimum number of one iteration at Bus 15 to a maximum number of six iterations at several buses.

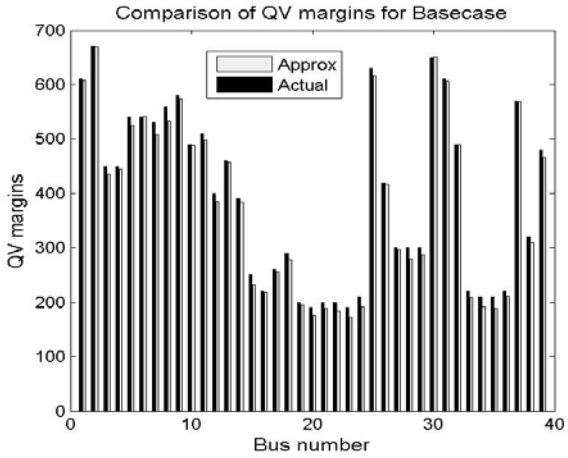

Figure 5.2 Comparison of Actual and Approximate QV margins for the base-case power-flow scenario

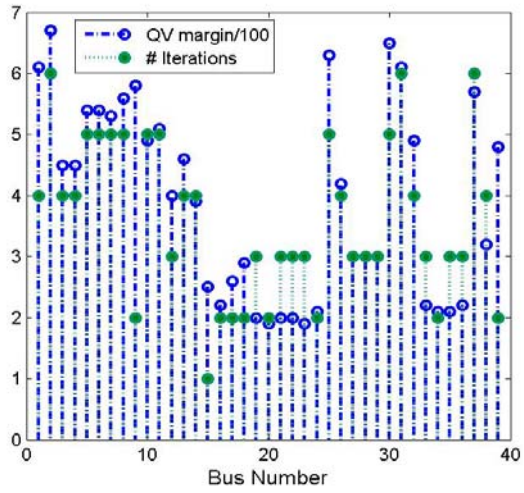

Figure 5.3 Plot of the number of iterations with the QV margins

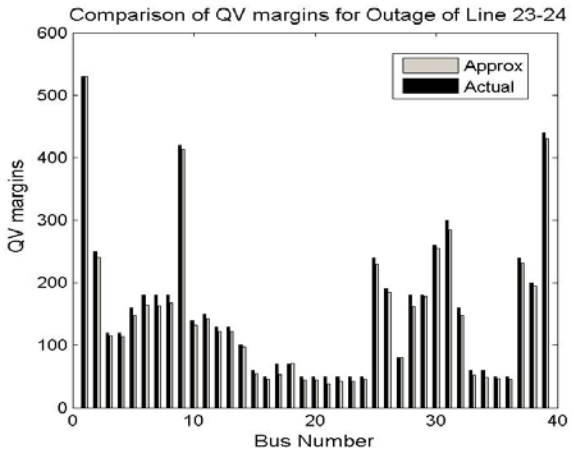

Figure 5.4 Comparison of QV margins for Outage of Line from Bus 23 to Bus 24

Figures 5.2 and 5.3 together highlight the strength of the proposed algorithm: The algorithm is fast in taking only a few iterations per bus to compute the approximate QV margin. However, the algorithm does not compromise on the accuracy of the QV margin computation over a wide range of values.

Figure 5.4 shows the comparison of the actual and approximate QV margins for the contingency case, Line outage of the transmission line connecting Buses 24 and 24. Again, the approximate values match very well with the actual values. As noted in Section 4, with the outage of the line from Bus 23 to Bus 24, the power system has been pushed close to voltage instability in the area near Bus 20 and the approximate method identifies the same voltage stressed region as the traditional repeated power-flow method. The error in QV margins ranges from the conservative difference of 18 MVAR at Bus 28 to the largest optimistic difference of 1 MVAR at Bus 18. These differences are very reasonable since the QV margins range from 50 MVAR at several buses near Bus 20 to 530 MVAR at Bus 1. The average in QV margins between the actual and approximate values is only 8 MVAR over the 39 buses. In Figure 5.3, the average number of iterations for the predictive method is 2.54. The algorithm takes mostly one or two iterations in the stressed region near Bus 20, while it takes a maximum of 4 iterations at several buses. Figure 5.5 shows a plot of the number of iterations of the fast predictive algorithm together with the QV margins at different buses for the outage case.

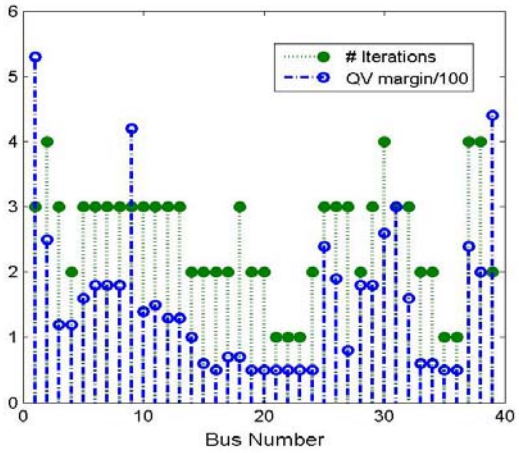

Figure 5.5 Plot of the number of iterations together with QV margins

Next, we test the system with another loading pattern shown in the appendix so that a different part of the system is stressed. Figure 5.6 shows the comparison of the actual and approximate QV margins and they match well. Interestingly, all the QV margins appear to be near or above 300 MVAR, which indicates that the system is operating away from the static voltage instability limits for the base-case scenario. The lowest QV margin is at Bus 28 with a value of 280 MVAR. The error between the actual and approximate QV margins range between a conservative error of +35 MVAR at Bus 3 to an optimistic error of –2 MVAR at Bus 38. The average error is 10 MVAR over the 39 buses. The average number of iterations for the fast algorithm is 5.08 which again indicates a small number of power-flow solutions to find the QV margins at each bus.

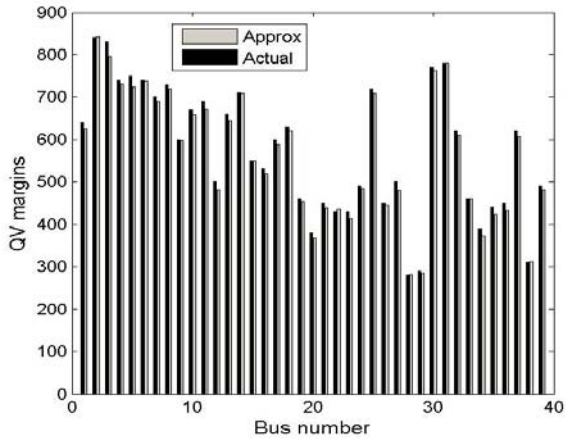

Figure 5.6 Comparison of QV margins for a different loading pattern

Figure 5.7 shows a comparison of the QV margins for the same case after the line outage of the transmission line connecting Buses 25 and 26. The results of the fast method match very well with their respective actual values of QV margins. After the line outage, the system has become vulnerable to voltage instability with near zero QV margins in the region near Bus 28. The lowest QV margin is 30 MVAR at Buses 26, 28, 29, and 38. The QV margins in the other parts of the system are still rather healthy with values above 150 MVAR. Because of computational constraints, the current industry practice is to carry out QV analysis at a pre-specified list of load buses. This example illustrates the problem with the approach. If none of these five buses 26, 27, 28, 29 and 38 with low QV margins were included in the QV study, the traditional limited QV analysis would have classified the system to be voltage secure after the line outage, whereas the system is actually on the verge of voltage instability. The fast algorithms proposed in the paper enable the QV analysis to be carried out all over the power system so that local voltage instability problems can be detected reliably and efficiently.

The fast algorithm takes an average of 3.72 iterations for the outage case. Interestingly, the predictive fast algorithm needs a small number of iterations, (one or two iterations in Figures 5.5 and 5.8) for the voltage stressed buses with low QV margins. Therefore, power-flow Jacobian based linear sensitivities can be used to further speed up the algorithm in place of the power-flow runs A and B in Figure 5.1. The second algorithm that is a faster version of the algorithm of Figure 5.1 is proposed in the next section.

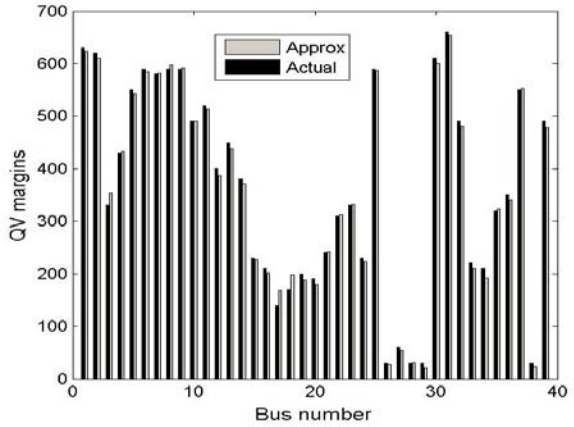

Figure 5.7 Comparison of QV margins after the outage of line from Bus 25 to Bus 26

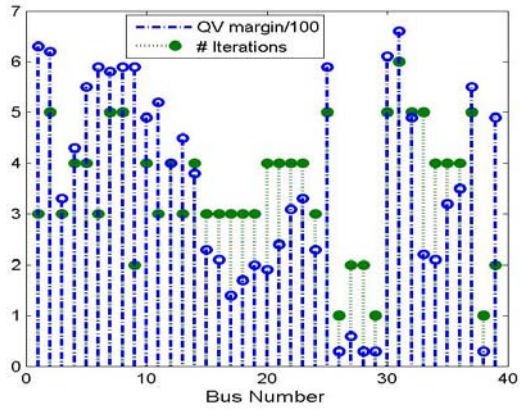

Figure 5.8 Plot of the number of iterations together with QV margins for the outage case

We consider the IEEE 300 bus test system next. The one-line diagram of the system is available at the University of Washington power system test archive website [6]. This is an excellent test system for voltage stability analysis because the system consists of some voltage stressed regions even for the base-case power-flow data.

By carrying out the traditional QV analysis, we find the QV margins range from 0 MVAR at several buses to 2040 MVAR at Bus 216. A comparison of the QV margins from the traditional method and the fast predictive algorithm for the 300 bus system is shown in Figure 5.9. The average error in MW margin over the 300 buses is only 5.78 MVAR. The maximum error occurs at Bus 220 (-96.7 MVAR, error on the conservative side), and at Bus 299 (+49.5 MVAR, error on the optimistic side). It should be pointed out that even standard power-flow calculations are very sensitive near Bus 299 in the 300 bus system because the group of buses near Bus 299 appears to represent a special subsystem. The average number of iterations is 4.18 for the fast algorithm, and the number of iterations ranges from 1 (fastest) to 14 (slowest). Significantly, the fast algorithm consistently finds the voltage critical buses with low QV margins as compared to the standard power-flow approach. The parameters of the fast algorithm are the same as for the 39 bus test system presented earlier in the section. By further tuning of the parameters for the 300 bus test system, the results could be improved, even though the results of the fast algorithm are quite reasonable without any tuning. Again, we want to emphasize that the mean value of the error in QV margin is only 5.78 MVAR over the 300 buses even though the average value of the actual QV margins themselves is rather high at 424 MVAR.

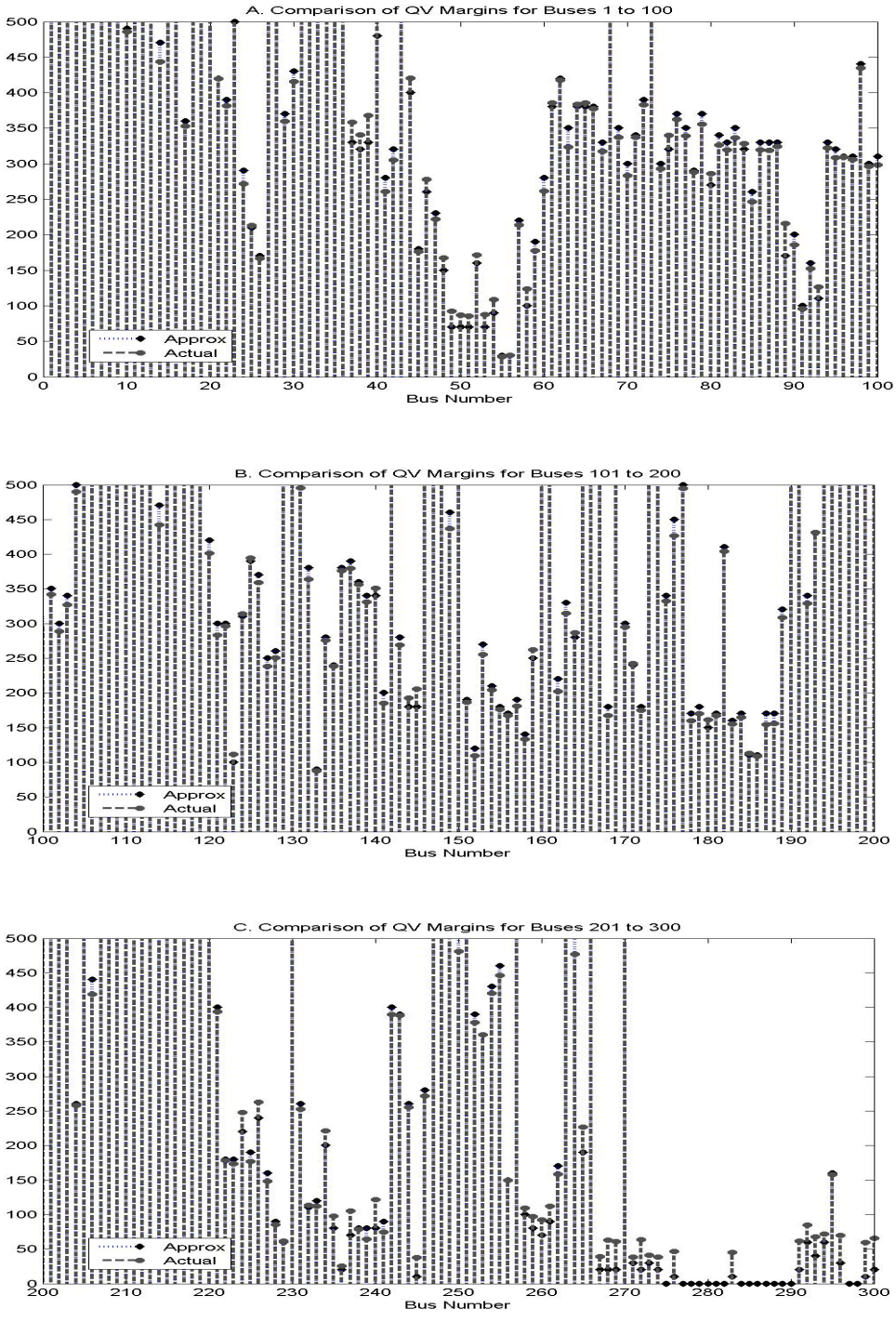

Figure 5.9 Comparison of QV margins for the IEEE 300 bus test system

6. **Direct Predictive QV Margin Calculator:**

The advantage of the fast predictive algorithm of Figure 5.1 in Section 5 is that the algorithm can be implemented using any standard power-flow engine. The algorithm processes the power-flow solutions (or the lack of existence of solutions) to predict when the generators reach their Q limits to accelerate the QV margin computation. The algorithm works well over a wide range of actual QV margin values from low margins to high QV margins, while taking only a few iterations at each bus.

In real practice, the critical question is to identify whether *any* of the buses has *low* QV margin for the *base-case* as well as after *all credible contingencies*. When the QV margin is above a certain value say 300 MVAR, it may not matter whether it is say 400 MVAR or 500 MVAR. On the other hand, the occurrence of low QV margins at any bus must be identified accurately and quickly. We propose a second "direct" algorithm in this section that uses the power-flow Jacobian together with the power-flow solution in the prediction step of Figure 5.1. The algorithm estimates the QV margin at all the load buses in the system *directly* in one step rather than carrying out multiple power-flow computations of the first algorithm.

6.1 Direct Algorithm flowchart:

The flowchart of the second algorithm is presented in Figure 6.1. Again, the algorithm as shown computes the QV margin at Bus i, where Q_{Li}^{margin} is defined as the difference of the static limit value of the reactive power load Q_{Li} from the base value Q_{Li}^{0}. In Figure 5.1, the fast predictive algorithm computes the generator reactive power Q_{Gi} sensitivities to the ε change in Q_{Li} by evaluating the two power-flow solutions A and B. In Figure 6.1, the direct predictive algorithm avoids finding the two power-flow solutions A and B of Figure 5.1 by directly computing the generator reactive power sensitivities Q_{Gi} from the power-flow Jacobian as shown in Appendix A. In Figure 6.1, the entire computation uses the starting power-flow solution say x^* and the initial full power-flow Jacobian shown in Appendix equation (A.3) evaluated at x^*.

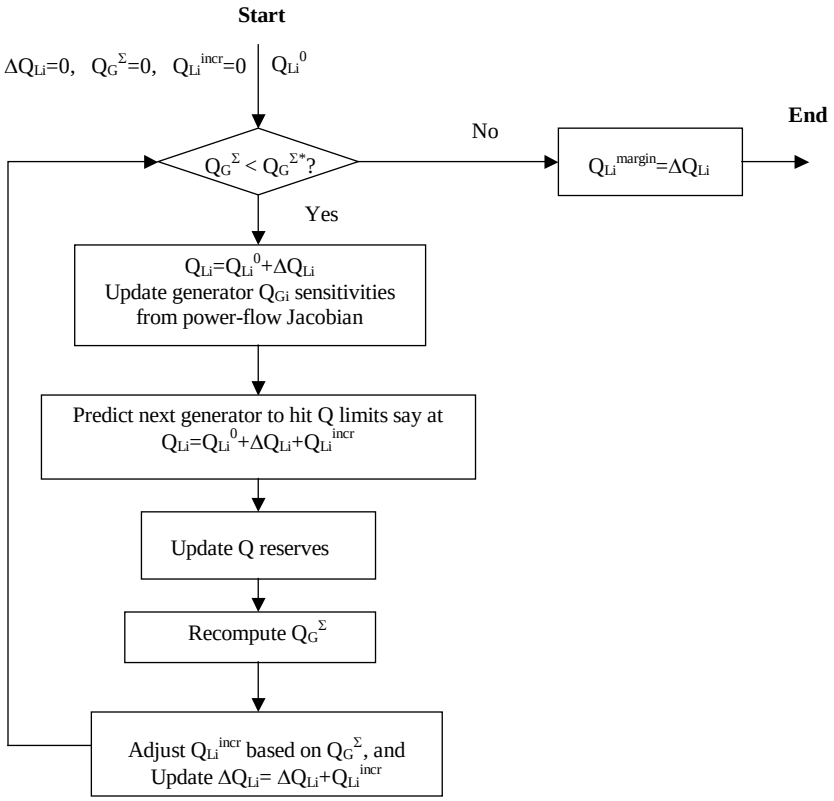

Figure 6.1 Flow-chart of the direct predictive QV margin calculator

6.2 Test results on the 39 bus system

Let us first apply the algorithm to the 39 bus New England test system base-case studied in Section 5.2. A comparison of the actual QV margins with the approximate QV margins computed by the direct algorithm is presented in Figure 5.2. The results of the direct algorithm match very well with the actual QV margins for the buses with low QV margins such as all buses near bus 20. This is the voltage stressed part of the system as discussed earlier, and the direct algorithm correctly identifies the low QV margin levels in this part of the system. Moreover, the direct algorithm results match well with the actual values over all the 39 buses. The largest optimistic error of 120 MVAR occurs at bus 9 that has a large healthy QV margin of 580 MVAR, and the largest conservative error of 84 MVAR occurs at bus 25 that again has a healthy QV margin of 630 MVAR. The average absolute error over the 39 buses is 29 MVAR, which is very reasonable given the fact that all the QV margins are computed directly from the generator reactive power reserves without any power-flow solutions.

The direct algorithm is especially accurate in identifying the buses with low QV margins. Let us suppose that we want to focus on those QV margins below 400 MVAR. Figure 6.2 can then be re-plotted as shown in Figure 6.3, which shows that the direct algorithm provides excellent results at all the buses. The average absolute error is only 8 MVAR with the largest conservative error of 26 MVAR at bus 15 to largest optimistic estimate of 37 MVAR at bus 27. The error between the actual and approximate QV margins is nearly zero for the voltage stresses buses near bus 20 as seen in Figure 6.3.

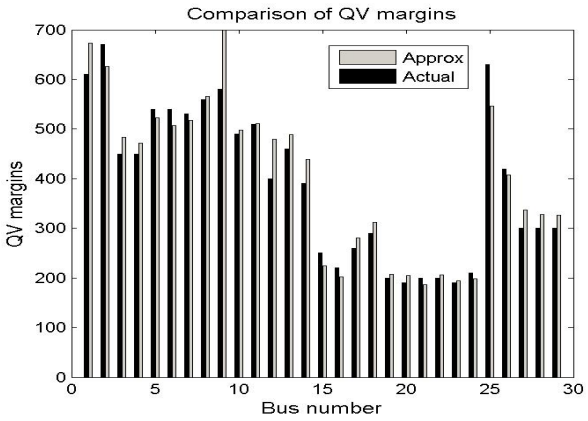

Figure 6.2 Comparison of Actual and Approximate QV margins for the base-case power-flow scenario

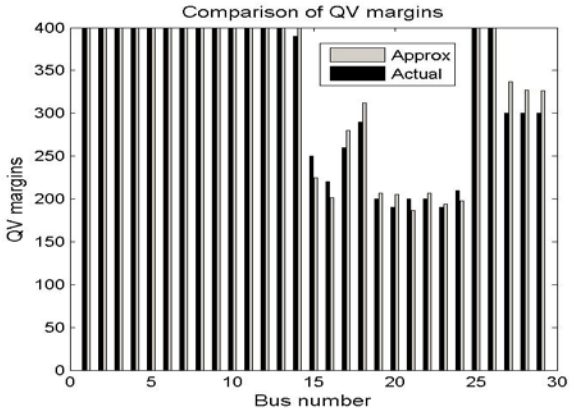

Figure 6.3 Another look at the comparison of QV margins

Let us consider the contingency case, namely, the outage of the transmission line from bus 23 to bus 24. A comparison of the actual and approximate QV margins for the outage case is presented in Figure 6.4. Again, we will assume that we ignore the QV margins and estimates above 400 MVAR. It is clear from Figure 6.4 that the direct algorithm provides excellent approximations of the actual QV margins at all buses. The average absolute error in the QV margin is only 11 MVAR over the 39 buses in Figure 6.4.

Next, we will study the second loading scenario like in Section 6.2. The comparison of the QV margins in Figure 6.4 again shows that the direct algorithm gives consistent estimates. The algorithm correctly identifies the buses with the lowest QV margins. Interestingly, even the lowest QV margin is 260 MVAR that is overestimated by the direct algorithm. The average absolute error in the QV margin estimation over the 39 buses in Figure 6.5 is 8 MVAR.

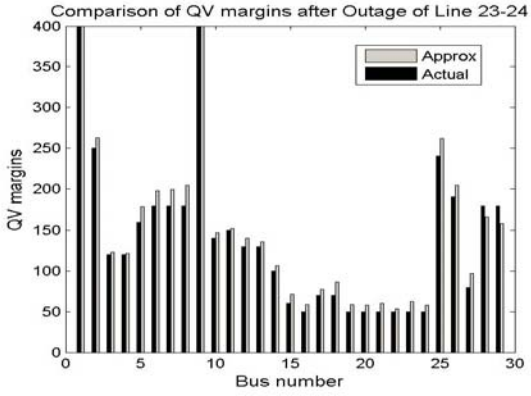

Figure 6.4 Comparison of QV margins for the line outage case

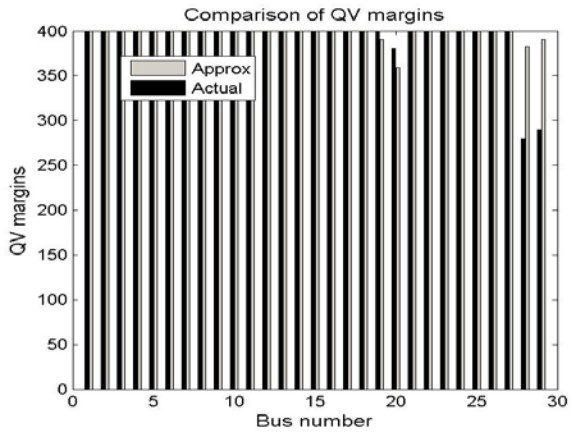

Figure 6.5 Comparison of QV margins for the different load scenario

We will study the outage of the line connecting buses 25 and 26 for the loading scenario in Figure 6.5. A comparison of the approximate and actual QV margins is presented in Figure 6.6. The direct algorithm corectly identifies the voltage stressed portion of the system near bus 29 with low QV margins. The average abolute error in the QV margin approximation in Figure 6.6 is 14 MVAR over the 39 buses.

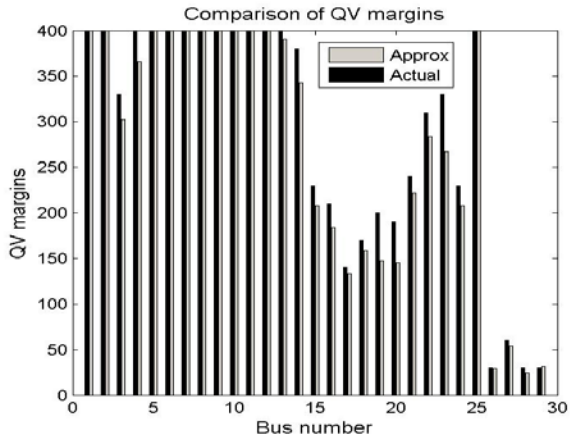

Figure 6.6 Comparison of QV margins for the outage of line from bus 25 to bus 26

The simulation results in this section show that the approximate values of QV margins computed by the direct algorithm in Figure 6.1 match very well with the actual QV margins over different loading conditions and for contingency cases. The direct method is therefore especially useful for identifying the voltage stressed parts of the system with low QV margins directly for the base-case and for contingency cases without having to solve repeated power-flow simulations.

7. Conclusions

The paper presents two new algorithms for fast assessment of voltage stability margins from power-flow models. Voltage stability margins are defined in terms of the QV margin, which is the distance between the current loading value and the limiting loading value on the QV diagram. Traditional approach requires a very large number of power-flow computations to compute the QV margin at any one bus. The two algorithms presented in the paper are shown to be much faster than the traditional approach, and still provide excellent approximations of the QV margins in test power-flow cases.

The main idea in the two algorithms is to monitor the reactive power reserves in an area, and predict when they will be depleted under loading changes. We show that for a given reactive power load change, the net change in reactive power outputs of area generators varies appreciably depending on system stress. Unusually large change in generator reactive power outputs to reactive load changes indicates proximity to voltage instability limits.

The first algorithm, Fast Predictive QV Margin Calculator, uses a predictive approach to estimate when the nearby generators will reach their reactive power maximum outputs under load increase to estimate the QV margins with a few power-flow computations. The algorithm thus monitors the generator reactive power outputs with loading changes and predicts when generators reactive power reserves will be depleted in a successive fashion.

The second algorithm, Direct Predictive QV Margin Calculator, combines the predictive approach of the first algorithm with sensitivities from the power-flow Jacobian matrices to provide direct estimates of QV margins at all buses. The algorithm requires only one power-flow solution and one evaluation of the power-flow Jacobian matrix to compute approximations of the QV margins at all system buses. The approximations match well with detailed simulation results for all the critical cases when the QV margins are small or zero. The second algorithm is primarily aimed at identifying the critical parts of the system that are weak with respect to voltage instability.

The second algorithm, Direct Predictive QV Margin Calculator, is very fast and is intended towards real-time implementation using synchrophasor measurements of the power system state. The power-flow Jacobian can be easily evaluated by knowing the system state and system topology from synchrophasor

measurements. The algorithm uses the power-flow Jacobian and real-time measurements of reactive power reserves again from synchrophasor measurements to provide fast estimates of QV margins at all the buses in the power system. The power-flow Jacobian entries can also be approximated from traditional SCADA measurements and the formulas for Jacobian entries are presented in [9],[10]. The algorithm provides a real-time estimate of the vulnerability of the power system towards voltage instability.

While the two algorithms stated in Sections 5 and 6 are illustrated for the calculation of QV margins (under reactive power load changes) in this paper, they can be easily extended to compute other types of static power-flow margins as well. For instance, the scaling of both real and reactive power loads at any one bus or multiple buses in an area can be used as measures of voltage security margins, and the simulation results will be illustrated in future publications.

The algorithms in Sections 5 and 6 can serve as the computational engines of a real-time voltage security controller. The controller can monitor the voltage security status of a part of a power system such as a critical load center, and can initiate suitable countermeasures to mitigate potential voltage instability whenever voltage instability problems are detected.

8. Acknowledgments

The author thanks Schweitzer Engineering Labs Inc., Pullman, WA for supporting the research work that is reported in this paper.

References

[1] Proceedings of Bulk Power System Voltage Phenomena: Voltage Stability and Security, Potosi, MO, 1988.
[2] Proceedings of Second Bulk Power System Voltage Phenomena: Voltage Stability and Security, Deep Creek Lake, Maryland, 1991.
[3] Proceedings of Third Bulk Power System Voltage Phenomena: Voltage Stability, Security and Control, Davos, Switzerland, 1994.
[4] J. Grainger and W. Stevenson, Power system analysis, McGraw-Hill, 1994.
[5] P. Kundur, Power system stability and control, McGraw-Hill, 1994.
[6] Power systems test case archive, Univ. of Wash., at http://www.ee.washington.edu/research/pstca/
[7] V. Venkatasubramanian and Y. Li, "Analysis of 1996 western American electric blackouts", Proc. IREP Symposium on Bulk power system dynamics and control-VI, Cortina d'Ampezzo, Italy, pp. 685-721, 2004.
[8] Matpower power-flow program, available at http://www.pserc.org
[9] Jingdong Su, A heuristic slow voltage control scheme for large power systems, Doctoral Dissertation, School of EECS, Washington State University, Pullman, WA, 2006.
[10] J. Su and V. Venkatasubramanian, "A hybrid on-line slow voltage control scheme for large power systems", Proc. IREP Symposium on Bulk Power System Phenomena, Charleston, SC, 2007.

Appendix A. Jacobian computations

In this Appendix, we will discuss how to compute the effect of variation of reactive power load at a bus say bus i on the generator reactive power outputs. Please refer to Section 3 for an introduction to the formulation of power-flow equations as used in this appendix.

Suppose the state variables are represented as x where

$$x = \begin{pmatrix} \delta_{PV} \\ \delta_{PQ} \\ V_{PV} \\ V_{PQ} \end{pmatrix} \qquad \text{(A.1)}$$

The corresponding power-flow equations from (3.1) and (3.2) are then stated as

$$\begin{pmatrix} p_{PV}(\delta_{PV},\delta_{PQ},V_{PQ}) \\ p_{PQ}(\delta_{PV},\delta_{PQ},V_{PQ}) \\ q_{PV}(\delta_{PV},\delta_{PQ},V_{PQ}) \\ q_{PQ}(\delta_{PV},\delta_{PQ},V_{PQ}) \end{pmatrix} - \begin{pmatrix} P_{PV} \\ P_{PQ} \\ Q_{PV} \\ Q_{PQ} \end{pmatrix} = \begin{pmatrix} 0 \\ 0 \\ 0 \\ 0 \end{pmatrix} \qquad \text{(A.2)}$$

Suppose a power-flow solution to the equations (A.2) is represented as x^*. Then, we can linearize (A.2) at x^* as follows.

$$\begin{pmatrix} \frac{\partial p_{PV}}{\partial \delta_{PV}} & \frac{\partial p_{PV}}{\partial \delta_{PQ}} & \frac{\partial p_{PV}}{\partial V_{PV}} & \frac{\partial p_{PV}}{\partial V_{PV}} \\ \frac{\partial p_{PQ}}{\partial \delta_{PV}} & \frac{\partial p_{PQ}}{\partial \delta_{PQ}} & \frac{\partial p_{PQ}}{\partial V_{PV}} & \frac{\partial p_{PQ}}{\partial V_{PV}} \\ \frac{\partial q_{PV}}{\partial \delta_{PV}} & \frac{\partial q_{PV}}{\partial \delta_{PQ}} & \frac{\partial q_{PV}}{\partial V_{PV}} & \frac{\partial q_{PV}}{\partial V_{PV}} \\ \frac{\partial q_{PV}}{\partial \delta_{PV}} & \frac{\partial q_{PQ}}{\partial \delta_{PQ}} & \frac{\partial q_{PQ}}{\partial V_{PV}} & \frac{\partial q_{PV}}{\partial V_{PV}} \end{pmatrix}_{|(x^*)} \begin{pmatrix} \Delta\delta_{PV} \\ \Delta\delta_{PQ} \\ \Delta V_{PV} \\ \Delta V_{PQ} \end{pmatrix} - \begin{pmatrix} \Delta P_{PV} \\ \Delta P_{PQ} \\ \Delta Q_{PV} \\ \Delta Q_{PQ} \end{pmatrix} = \begin{pmatrix} 0 \\ 0 \\ 0 \\ 0 \end{pmatrix}$$

(A.3)

Next, let us assume that we want to compute the effects from a small perturbation of $+\varepsilon$ in Q_{Li} on generator reactive power outputs Q_{Gi}. Assuming that ε is sufficiently small, the net effect on Q_{Gi} from the load change $\Delta Q_{Li} = +\varepsilon$ can be computed from linearized equations (A.3). First, note that $\Delta Q_{PQi} = -\varepsilon$ and the

remaining entries of $\Delta Q_{PQ} = 0$. We will assume that the active power loads do not change, which implies that $\Delta P_{PQ} = 0$. Accordingly, we will also assume that the active power generations do not change, and therefore, $\Delta P_{PV} = 0$ as well. Moreover, by assumption, the PV buses remain constant which implies that $\Delta V_{PV} = 0$. Based on the observations above, the changes in ΔQ_{PV} can then be calculated as follows:

$$\Delta Q_{PV} = \left(\frac{\partial q_{PV}}{\partial V_{PV}}\right)_{|(x^*)} \left(\frac{\partial q_{PQ}}{\partial V_{PQ}}\right)^{-1}_{|(x^*)} \Delta Q_{PQ} \qquad \text{(A.4)}$$

In the implementation of the direct predictive algorithm in Section 6, we will assume that the starting power-flow solution and the full Jacobian matrix in equation (A.3) at this power-flow solution are available at the beginning of the calculations, In each step in the algorithm shown in Figure 6.1, the algorithm moves one generator bus from being a PV bus to a PQ bus by modifying the state vector x in (A.1) appropriately. The later computations for (A.4) are carried out by using the same power-flow solution values from x^* and by using the appropriate entries of the original Jacobian matrix in (A.3) according to the structure of PV and PQ vectors at that time. The assumptions are shown to work well in the simulations reported in Section 6.

Next let us consider the more general case of small perturbations in any of the real and reactive power loads, and we want to compute the corresponding changes in generator real and reactive power outputs. That is, we assume that ΔP_{PQ} and ΔQ_{PQ} are specified. We want to compute ΔP_{PV} and ΔQ_{PV}. First, we assume that the changes ΔP_{PQ} are small in magnitude so that the corresponding changes in line losses can be ignored. Then, active power conservation implies that

$$\sum_i \Delta P_{PQ_i} = \sum_i \Delta P_{PV_i} \qquad \text{(A.5)}$$

The individual changes in ΔP_{Pvi} can then be computed from the sum of net active load power changes in (A.4) by using one of the standard assumptions:

a) generator active power outputs change proportional to their active power capacities (governor power-flow assumption);
b) active power outputs of a few specific "slack" generators pick up the net load power change (AGC power-flow assumption);
c) active power outputs of the generators are recomputed using some form of economic dispatch computations.

By assuming any one of the three formulations above, changes in the active power outputs of generators can be computed and hence, we can assume that ΔP_{PV} is known as well. The problem thus reduces to finding $\Delta Q_{PV,}$ which can be solved from the Jacobian equation (A.3) by recognizing all the known quantities and by simple algebraic manipulations. Again, we note that $\Delta V_{PV} = 0$ in (A.3) which allows us to solve the remaining state variable changes as follows.

$$\begin{pmatrix} \Delta\delta_{PV} \\ \Delta\delta_{PQ} \\ \Delta V_{PQ} \end{pmatrix} = \begin{pmatrix} \frac{\partial p_{PV}}{\partial \delta_{PV}} & \frac{\partial p_{PV}}{\partial \delta_{PQ}} & \frac{\partial p_{PV}}{\partial V_{PV}} \\ \frac{\partial p_{PQ}}{\partial \delta_{PV}} & \frac{\partial p_{PQ}}{\partial \delta_{PQ}} & \frac{\partial p_{PQ}}{\partial V_{PV}} \\ \frac{\partial q_{PV}}{\partial \delta_{PV}} & \frac{\partial q_{PQ}}{\partial \delta_{PQ}} & \frac{\partial q_{PV}}{\partial V_{PV}} \end{pmatrix}^{-1}_{|(x^*)} \begin{pmatrix} \Delta P_{PV} \\ \Delta P_{PQ} \\ \Delta Q_{PQ} \end{pmatrix} \qquad \text{(A.6)}$$

Next, ΔQ_{PV} can be solved as follows.

$$\Delta Q_{PV} = \left(\frac{\partial q_{PV}}{\partial \delta_{PV}} \quad \frac{\partial q_{PV}}{\partial \delta_{PQ}} \quad \frac{\partial q_{PV}}{\partial V_{PV}}\right)_{|(x^*)} \begin{pmatrix} \Delta\delta_{PV} \\ \Delta\delta_{PQ} \\ \Delta V_{PQ} \end{pmatrix} \qquad \text{(A.7)}$$

The algorithms in Figures 5.1 and 6.1 can be readily modified to compute the static limit margins in the sense of scaling active and reactive power loads in any number of specified load buses by using the same principles in Figures 5.1 and 6.1 respectively.

BACK TO THE TABLE OF CONTENTS